IEEE Access
Multidisciplinary ⋮ Rapid Review ⋮ Open Access Journal

Received 28 January 2024, accepted 12 February 2024, date of publication 19 February 2024, date of current version 27 February 2024.

Digital Object Identifier 10.1109/ACCESS.2024.3367435

RESEARCH ARTICLE

Classification of Floor Materials Using Piezoelectric Actuator–Sensor Pair and Deep Learning for Mobile Robots

JIYONG MIN, JISUNG PACK, HEON ICK PARK, AND YOUNGSU CHA, (Senior Member, IEEE)
School of Electrical Engineering, Korea University, Seoul 02841, Republic of Korea

Corresponding author: Youngsu Cha (ys02@korea.ac.kr)

This work was supported by the National Research Foundation of Korea (NRF) Grant funded by the Korea Ministry of Science and ICT (MSIT) under Grant 2022M3C1A3098746.

ABSTRACT Analyzing floor surface materials is critical for controlling the motion and tasks of mobile robots. In this study, we propose a novel method for classifying floor materials for indoor mobile robots using a piezoelectric actuator–sensor pair and deep learning. This method can classify the floor properties itself with isolated sensing system while the mobile robot is moving. The piezoelectric pair is a thin-film type. It consists of an actuator and a sensor. The sensing pair is positioned at the bottom of the robot. When the robot moves forward, the sensing part collects the electrical responses from the actuator. Since one-dimensional data is collected through the piezoelectric actuator-sensor pair, the size of the system is small and the data processing speed can be reduced. Using this mechanism, experiments were conducted to classify various materials of floor surfaces in indoor environments. The sensing data were processed by fast Fourier transform, high-pass filter, polynomial fitting, and sampling to be used as inputs for machine learning of the classification model. Specifically, the trained model achieved a high accuracy of 95.4%. In addition, the training data were verified using the k-means clustering method. Moreover, the effect of the physical properties on the sensor data was analyzed to investigate the relationship between the materials and the sensing outputs.

INDEX TERMS Piezoelectric sensor, material classification, mobile robot, neural network.

I. INTRODUCTION

Robots for household and daily tasks are attracting increasing attention owing to their convenience and technological development [1]. In particular, mobile robots provide safe and stable services by moving around and performing desired tasks, such as cleaning or delivery [2], [3]. To accomplish these tasks appropriately, they must recognize the surrounding environment in detail. For example, robot cleaners obtain spatial data to reconstruct maps of the surrounding spaces and avoid obstacles [4], [5], [6]. In addition, mobile robots require more complex information about floors to prevent accidents, such as drops or slips [7], [8], [9]. Thus, the floor must be analyzed when manipulating mobile robots. In this study, we focused on recognizing floor materials to aid robot locomotion and manipulation using various types of floor information.

Clearly, the floor material directly affects the motion of the robot because locomotion is related to the interaction between the mobile robot and the ground. For instance, the slip of a robot is caused by low friction on its wheels or by a carpet that is not firmly fixed on the floor. In addition, the task types of the robots depend on the floor material. For robot cleaners, an appropriate cleaning method can be selected for different floor types [10]. Similarly, diverse methods have been proposed for recognizing floor materials, including laser scanning [11], image training [12], [13], and vibration analysis [14], [15], [16]. A common scheme in these conventional approaches is to identify the roughness of a surface. However, it is difficult to explain that topographic

The associate editor coordinating the review of this manuscript and approving it for publication was Yogendra Kumar Prajapati.

data reflect the properties of the floor. Thus, we suggest a novel method using a piezoelectric actuator–sensor pair as a new approach for the direct analysis of the floor surface by exploiting the physical properties of materials.

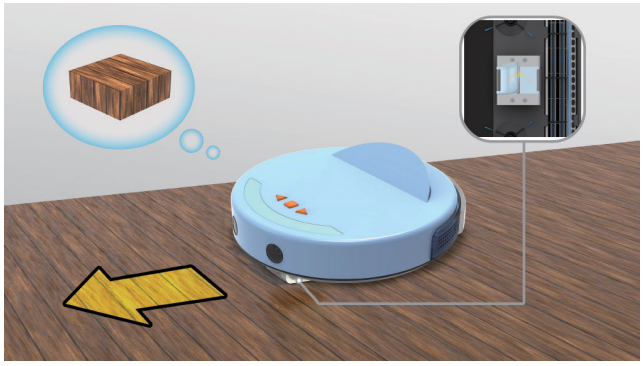

FIGURE 1. Concept image illustrating material classification of the ground using a mobile robot and piezoelectric sensor module.

The piezoelectric materials used in this study were made of polyvinylidene fluoride (PVDF) films [17], [18], [19], [20]. PVDF is soft and light; hence, it has been applied to a sensor array to identify the topography of facing surfaces, like artificial skin [21], [22], [23], [24]. In addition, a sensing method based on PVDF films was used for object classification by exploiting vibration feedback [25], [26], [27]. With these advantages of piezoelectric materials, we propose one of the applications by using a piezoelectric actuator–sensor pair fabricated with PVDF films to classify properties of the floor. Unlike recognizing the terrain on the floor surface, our method distinguishes the floor properties while the mobile robot is moving. This mobile robot is designed with an independent sensor system inside the robot to collect sensor data and even determine floor materials on its own. The distinguishing floor properties ensure that mobile robots can move safely and perform optimal tasks according to their surrounding environments. In addition, since the weight and volume of the pair were light and thin, the pair is useful when adapting to small mobile robots. Furthermore, as the sensor data was one-dimensional data about voltage variations over time, data processing is faster than two or three-dimensional data and takes up less data storage space. To provide mobile robots with reliable information about the floor, deep learning was used with the piezoelectric actuator–sensor pair. Specifically, the actuator–sensor pair was in contact with the floor while the mobile robot moved. The actuator applied mechanical and electrical stimuli to the floor, and the sensor collected feedbacks through the floor as responses related to the physical properties of floor materials. Extensive raw data were collected by repeating the experiment. Subsequently, the raw data were processed, and a training data was prepared. The dataset was used in learning phase of an artificial neural network, and a classification model for recognizing the floor material was constructed.

This paper is organized as follows: In Section II, experimental methods, including the fabrication process of a piezoelectric actuator–sensor pair, operating mechanism, and structure of the classification model, are described. In Section III, a sensor response analysis with the physical properties of floor materials and the results of the classification model training are presented. Finally, the conclusions are summarized in Section IV.

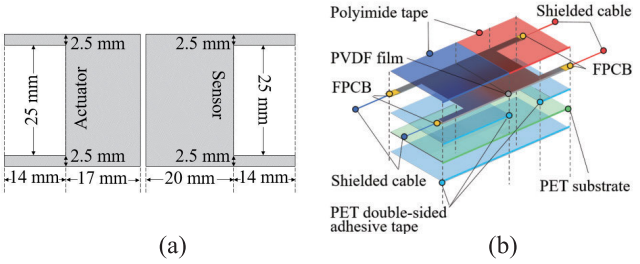

FIGURE 2. Design of the actuator–sensor pair: (a) schematics and (b) layer configuration. The red part is the actuator, and the blue part is the sensor.

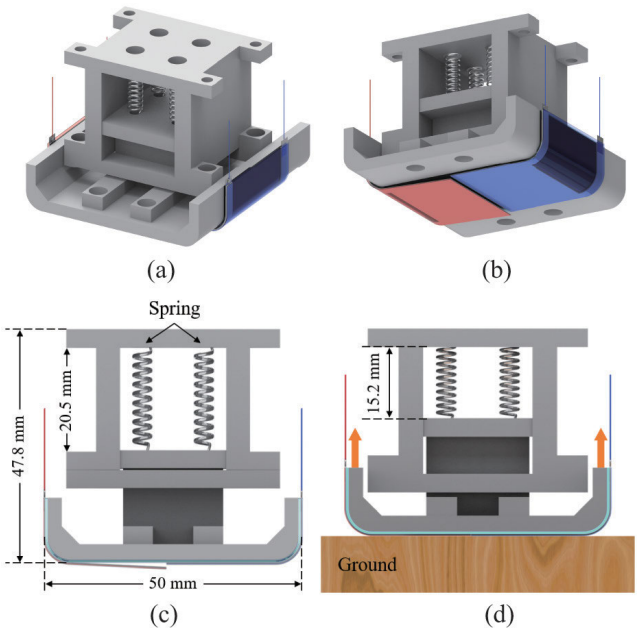

FIGURE 3. Illustration of the suspension and its mechanism: (a) high-angle view, (b) low-angle view, (c) side view of the initial state, and (d) side view when laid on the floor.

II. METHOD

A. ACTUATOR–SENSOR PAIR FABRICATION

An actuator–sensor pair structure was used to obtain ground information. To fabricate the structure, 110 µm- and 28 µm-thick PVDF films (Measurement Specialties, Inc., USA) were used for the actuator and sensor part, respectively. As the PVDF film has a low Young's modulus and thin thickness, it is effective for removing the resonance-induced effect from vibration and increasing the sensitivity of the sensor [28]. Also, these PVDF characteristics can help the piezoelectric

actuator generate bigger vibrations toward the floor to improve the performance of the classification. These films were cut into shapes as shown in Fig. 2(a). Using a sampling multimeter (DMM7510; Keithley Instruments, Inc., USA), the capacitances of the actuator and sensor were measured as 0.5961 nF and 1.768 nF, respectively. Flexible printed circuit boards (FPCB) soldered with cables were attached to the actuator–sensor pair using carbon conductive adhesive tape (Nisshin EM Co., Ltd., Japan). In addition, polyethylene terephthalate (PET) film (thickness: 100 µm; Saehan Co., Ltd., Korea) was cut into a size of 65 mm × 30 mm (width × length) for a flexible substrate. Subsequently, double-sided PET film tape (thickness: 50 µm; Saehan Co., Ltd., Korea) was used to enable PVDF films to adhere to one side of the PET substrate, and the PVDF films were covered by polyimide tape (3M, Inc., USA) for protection. Fig. 2(b) shows the overall schematic of the tactile sensor fabrication.

B. EXPERIMENTAL SCHEME AND DATA PROCESSING

To install the sensing pair under the mobile robot, a curved panel was 3D-modeled and printed using a 3D printer (3DWOX 2X, Sindoh Co., Ltd., Korea) with polylactic acid (PLA) material. The panel was designed to have a curved shape to prevent damage to the PVDF films when sliding on the floor. In addition, the suspension was 3D-printed, as shown in Fig. 3. The fabricated pair was attached to a curved panel of the suspension. The suspension maintained the pair at the bottom of the mobile robot in contact with the floor under limited pressure from the floor. This simple suspension format allowed the size of the system to be dramatically reduced by keeping the actuator-sensor pair in close contact with the floor. Figs. 3(a), 3(b), and 3(c) illustrate the high- and low-angle views and side view of the suspension combined with the pair, respectively. In addition, Fig. 3(d) shows the working process of the suspension when the mobile robot is placed on flat ground.

To control the mobile robot and the pair, three controller boards were used: a main computer (Jetson Nano; NVIDIA, Inc., USA), function generator/analog-to-digital converter module (FAM), and an electronic control unit (ECU; OpenCR 1.0; ROBOTIS, Inc., Korea). The main computer was connected to the ECU and FAM to send driving control signals and collect sensor data. The ECU was responsible for controlling the movement of the mobile robot. Additionally, the FAM consisted of a microcontroller unit (MCU; TMS320F28377S-100 module; Syncworks, Inc., Korea), USB serial communication unit (FT2232H MINI module; FTDI Co., Ltd., United Kingdom), switching mode power supply, voltage converter, sine generator, and additional circuits for the sensor module. The piezoelectric actuator–sensor pair was connected to the FAM through cables. In this way, the main computer and sensor system are built into one robot, allowing the robot to independently perform sensor system and floor material classification without external intervention. The configuration of the mobile robot is shown in Fig. 4.

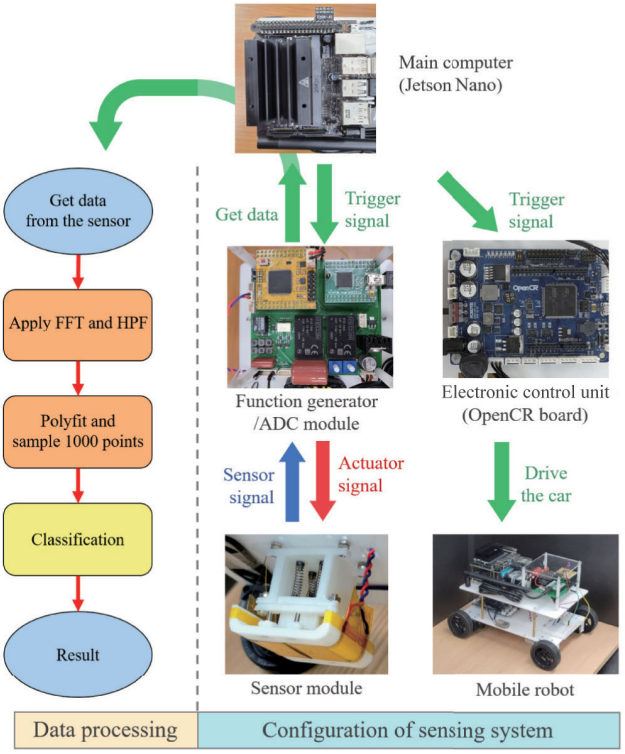

FIGURE 4. Configuration of the sensing system and data processing.

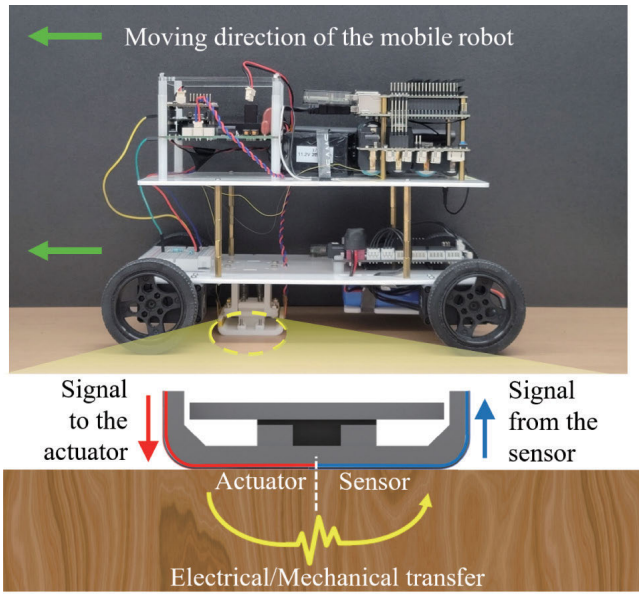

FIGURE 5. Operation mechanism of the piezoelectric actuator–sensor pair system.

Specifically, as the first step in data collection, the main computer triggered signals to the ECU and FAM. The mobile robot then moved forward at a speed of 10 cm/s for 4 seconds. Simultaneously, the MCU activated the FAM circuit to operate the actuator with a high-voltage sinusoidal input and acquire electrical responses from the sensor. The FAM generated an alternating voltage of 200V amplitude with

an offset voltage of 200V. The frequency of the sinusoidal input was swept from 100 Hz to 1 kHz for approximately 2.3 seconds. For the sensing component, the sampling frequency of the MCU was selected to be 25 kHz. The sensing was terminated at the end of the actuator sweep, resulting in 57687 data points.

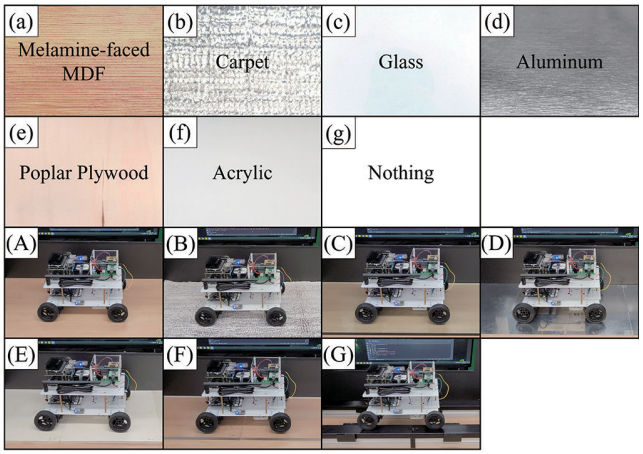

FIGURE 6. Pictures illustrating the selected floor materials and tests for data collection: (a)-(A) melamine-faced MDF, (b)-(B) carpet, (c)-(C) glass, (d)-(D) aluminum, (e)-(E) poplar plywood, (f)-(F) acrylic, and (g)-(G) nothing.

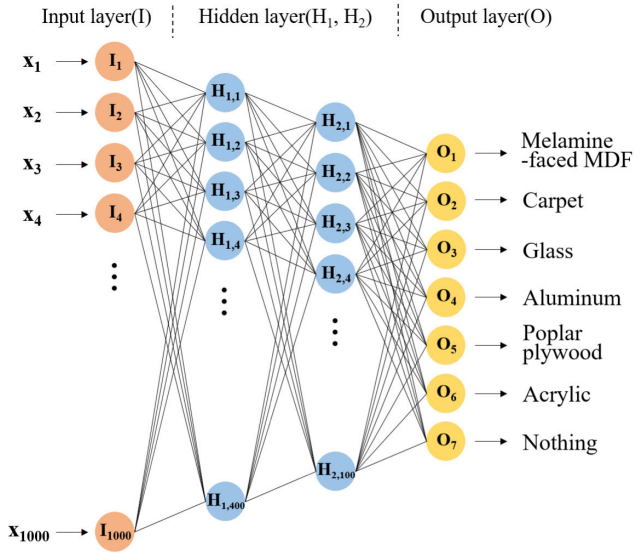

FIGURE 7. Architecture of dense neural network used for classification.

During the operation, the actuator generated mechanical vibrations owing to the piezoelectric effect of the PVDF film, as shown in Fig. 5. Subsequently, as the vibrations were transmitted to the sensor through the substrate and floor, electrical responses were measured from the sensor. The bottom electrodes of the actuator and sensor function as capacitances. The plain-shaped floor acted as a dielectric substance between the electrodes; hence, the capacitance depended on the floor material [29]. Therefore, the floor acted as a medium for electrical/mechanical transfer during

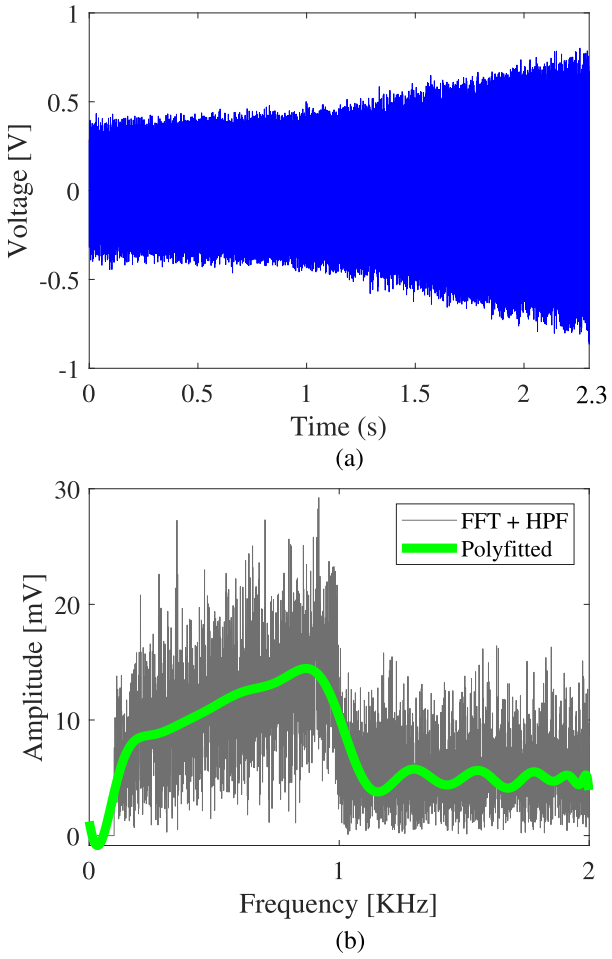

FIGURE 8. Time and frequency responses of the melamine-faced MDF when sweeping the input signal of the actuator: (a) Time responses of the sensor output, and (b) frequency responses of the sensor. The grey and green line represent the HPF-passed data with FFT applied and the 30th-degree polyfitted result of the grey line, respectively.

operation. Using these two mechanisms, the sensor collected information from the floor panels.

The collected sensor data were transmitted from the MCU to the main computer. Subsequently, the data were processed using the main computer as shown in Fig. 4. A fast Fourier transform (FFT) was applied to the raw data, and values corresponding to the range of 0–2 kHz were obtained. Moreover, a high-pass filter (HPF) with a cutoff frequency of 100 Hz was used to reduce the noise. Finally, the data were polyfitted with a 30th degree polynomial and obtained 1000 equally spaced samples from 0 to 2 kHz. Polynomial fitting was applied to reduce noise and extract the overall tendency. After polyfitting, the samples were used as training input in the neural network to classify the material set.

Fig. 6 shows the floor material set and their tests. Specifically, six flat panels made of different materials that were usually observed in indoor environments and "nothing" were selected. "Nothing" implied that no contact surface existed owing to the floating of the mobile robot. The

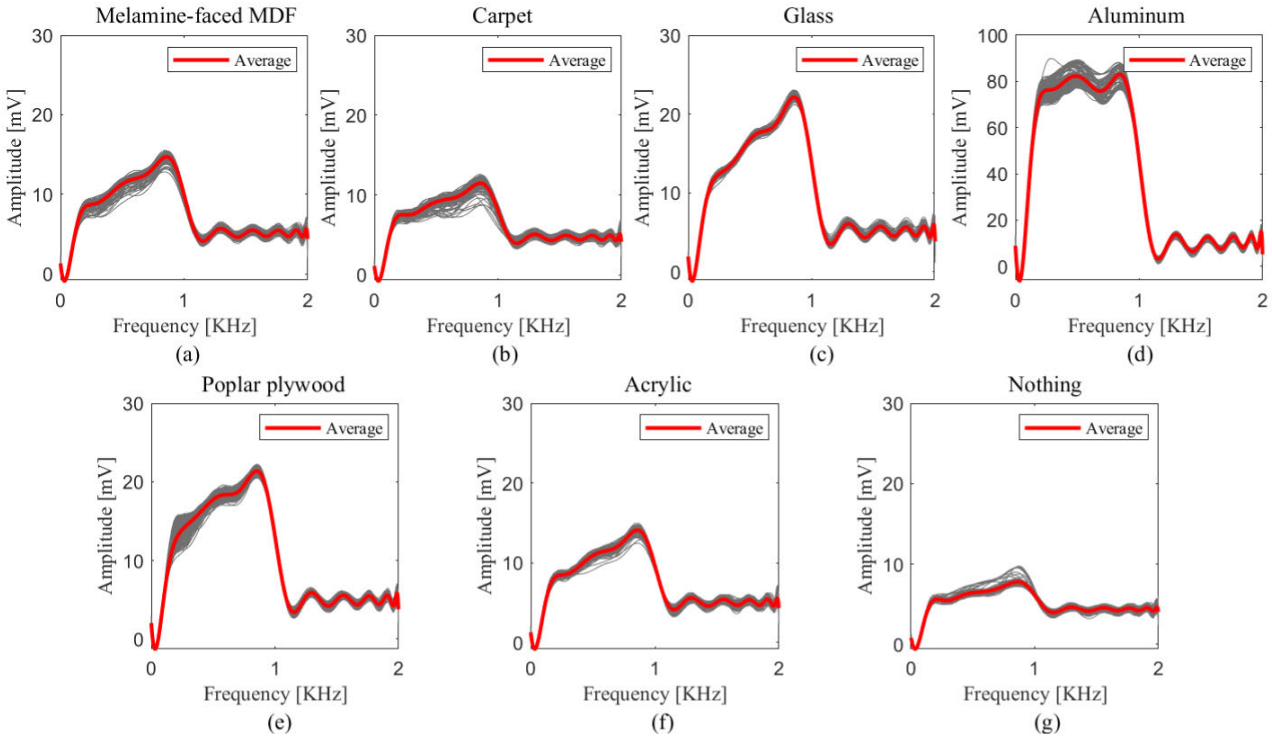

FIGURE 9. Frequency spectra for each surface material used in the training classification model. Grey lines in each plot correspond to 240 input data for machine learning. Red lines represent average spectrum of the input dataset. (a) Melamine-faced MDF, (b) carpet, (c) glass, (d) aluminum, (e) poplar plywood, (f) acrylic, and (g) nothing.

experiments were repeated and sensor data were collected for these seven types.

C. NEURAL NETWORK FOR CLASSIFICATION

In this setting, 240 experiments were conducted for each floor condition to obtain model training, test, and validation data inputs. In total, 1680 data were collected. These data were preprocessed and collected to form a dataset D:

$$\mathbf{D} = \{(\mathbf{x}_n, \mathbf{y}_n), n = 1, \ldots, 1680\}, \tag{1a}$$

$$\mathbf{x}_n = [x_{n,1}, x_{n,2}, \ldots, x_{n,1000}]^T, \tag{1b}$$

$$\mathbf{y}_n = [y_{n,1}, y_{n,2}, \ldots, y_{n,7}]^T. \tag{1c}$$

where $\mathbf{D}$ represents an input dataset for supervised machine learning, $\mathbf{x}_n$ represents a vector of the nth processed sensor data, and $\mathbf{y}_n$ represents a categorical ground-truth vector of the class number of the surface material corresponding to $\mathbf{x}_n$. This dataset was used to train the classification models. A dense neural network (DNN) was adopted as a classifier for floor surface materials. Fig. 7 demonstrates the architecture of the proposed classification model. Specifically, a multilayer perceptron (MLP) layer consisted of a combination of input/hidden layers with a size of 1000-400-100 and dropout layers with a scale of 0.2. The dropout layers prevented overfitting by eliminating unnecessary nodes [30], [31], [32], [33]. Additionally, an L2 regularizer with a regularization rate of 0.002 was applied to each input/hidden layer. The L2 regularizer prevented overfitting of the model to the training data by assigning penalties to data with high variance [32], [33], [34], [35]. To prevent training from overfitting, early stopping by monitoring the validation loss after 1000 epochs was applied [36], [37]. To train the classification model, supervised learning was executed for 4000 epochs using dataset $\mathbf{D}$. The ratio of the training, test, and validation sets was 4:1:1, and they were separated after the mixing data randomly. The DNN was implemented using the Keras API (version 2.6.0) on Python 3.8.8, and the model was trained on a desktop computer with a CPU (Intel Core i9–10900 CPU, Intel, Inc., USA), RAM (DDR 43 200 MHz 32 GB RAM, Samsung Electronics, Inc., Korea), and GPU (GeForce RTX 3070 GPU, NVIDIA, Inc., USA). After model training, the model was ported to the main computer of the mobile robot.

III. RESULT AND DISCUSSION

A. DATA AND MATERIAL ANALYSIS

The collected sensor data were processed based on the experiments described in the previous section. Fig. 8 shows an example of the sensor data and processing mechanism from the experiment conducted on the melamine-faced MDF. Although the amplitude of the input signal remained constant while sweeping the frequency, the responses increased with time and frequency. In addition, the frequency responses, as shown in Fig. 8(b), presented dominant values in the range of 100 Hz to 1 kHz caused by the voltage sweep. Furthermore, a small amplitude appeared in range of 1 kHz to 2 kHz by the

effect of the harmonic terms. Moreover, low-frequency power noises were effectively removed using an HPF with a cutoff frequency of 100 Hz. Consequently, the polyfitted graph represented the overall shape of the frequency responses.

Through data processing, 240 processed data for each surface material were synthesized and plotted with the average values, as shown in Fig. 9. Because the frequency sweep of the electrical signals to the actuator was performed in the range of 100 Hz to 1 kHz, dominant values appeared with an increasing tendency for every material in the corresponding range of the frequency domain, whereas aluminum showed a slight decline from 500 Hz to 700 Hz. In addition, the maximum points for each material occurred at approximately 850 Hz. The maximum values (V_{max}) and corresponding frequencies (f_{max}) are presented in Table 1. Aluminum had the largest V_{max} of 83.08 mV, followed by glass, poplar plywood, melamine-faced MDF, acrylic, carpet, and nothing in descending order. The V_{max} of aluminum was 2.75 times higher than that of glass and was remarkably high among the materials. Moreover, f_{max} did not vary with the material.

To investigate the differences in V_{max} with the floor materials, the correlations between the physical properties of the materials and V_{max} were analyzed. As mentioned regarding the mechanism of sensor operation, mechanical and electrical factors can affect the sensor data. In this context, the physical properties of the floor panels were organized in view of the floor with two layers: the surface and substrate core. We noted that the floor could have a coating layer and a layer below it in these case. We assumed that the surface materials acted as dielectric substances between the electrodes of the actuator and the sensor [29]. Thus, the electrical properties might be key factors to consider. Meanwhile, we focused on the mechanical properties of the core materials because mechanical vibration can propagate from the source in every direction with attenuation [45]. In the context, resistivity (ρ_r), dielectric constant (ϵ_r) of surface materials, and Young's modulus (E) of core materials were surveyed. The properties of six floor materials are presented in Table 1. Using these values, Fig. 10 shows the relationship between V_{max} and each property.

As shown in Fig. 10(a), V_{max} showed a decreasing tendency according to the resistivity. Moreover, as the resistivity increased to that of insulators ($10^{10}\,\Omega\cdot$m approximately), it was stabilized to low value. In contrast, V_{max} increased linearly as the dielectric constant increased, as shown in Fig. 10(b). From Fig. 10(a) and (b), the dielectric constant had a greater effect on the maximum sensor voltage than the resistivity, except for the case of aluminum. The reason is presumed to be that when the floor material is a non-conductor, a capacitance relationship can occur between the actuator part, the sensor part, and the floor [29]. Otherwise, in the case of aluminum, it was speculated that the floor acted as a wire connecting the electrodes of the actuator and the sensor, causing large voltage changes. Consequently, we inferred that materials with extremely small resistivities,

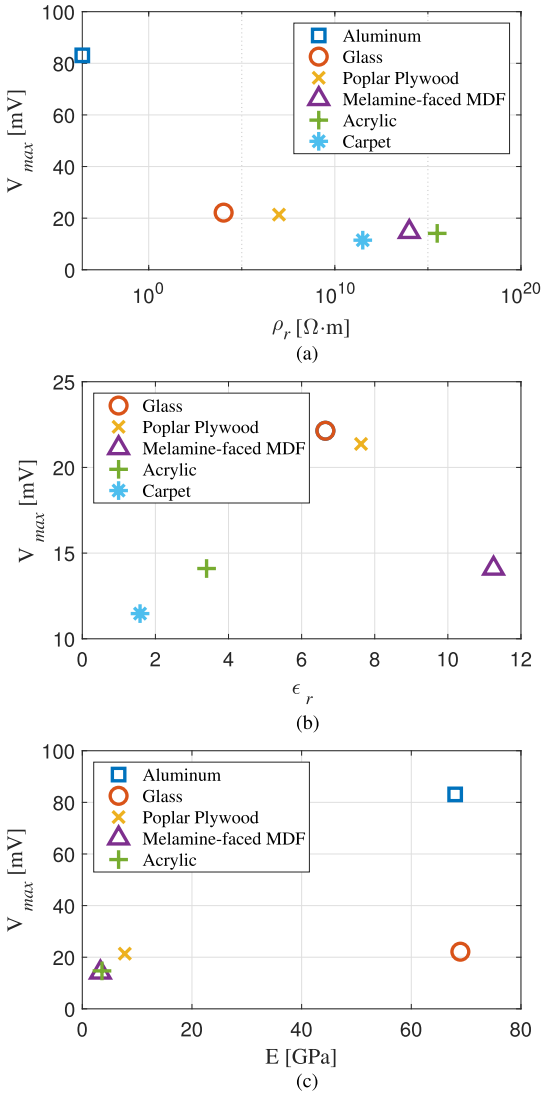

FIGURE 10. Distribution of the maximum voltages (V_{max}) according to (a) resistivity (ρ_r), (b) dielectric constant(ϵ_r), and (c) Young's modulus (E). Blue squares correspond to aluminum, orange circles to glass, yellow crosses to poplar plywood, purple triangles to melamine-faced MDF, light green plus signs to acrylic, and light blue asterisks to carpet.

such as conductors, or those with high permittivity result in a high V_{max}. However, for the melamine-faced MDF, its V_{max} did not correspond with linearity, as shown in Fig. 10(b). Melamine-faced MDF was the only floor panel comprising two layers of different materials in the classification set. This might be attributed to different trends.

In Fig. 10(c), two remarkable features are shown. Glass and poplar plywood had values of Young's modulus that were 10 times different but showed similar values of V_{max}. In contrast, glass and aluminum had similar Young's moduli, but V_{max} significantly differed. When the actuator generated vibrations toward the floor, the piezoelectric sensor detected vibrations transmitted to the floor [28], [46], [47]. From the sensor data, the topography of the floor could be identified. However, in Fig. 10(c), the maximum voltages of the sensor output are nearly the same for each insulator material even

TABLE 1. Electrical response results and properties of the surface materials.

	Melamine-faced MDF	Carpet	Glass	Aluminum	Poplar Plywood	Acrylic
V_{max} (mV)	14.70	11.47	22.14	83.08	21.37	14.10
f_{max} (Hz)	858	858	858	858	852	858
Surface material	Melamine	Cotton	Glass	Aluminum	Poplar Plywood	Acrylic
ϵ_r	6.5 – 16.0 [38]	1.30 – 1.86 [39]	4.7 – 8.6 [40]	-	6.62 – 8.63 [41]	2.8 – 4 [38]
ρ_r (Ω·m)	1.0×10^{12} – 1.0×10^{16} [38]	1.0×10^{7} – 1.0×10^{16} [42]	8.6×10^{3} – 1.31×10^{4} [40]	2.7×10^{-4} [38]	9.9×10^{6} – 1.02×10^{7} [41]	1.0×10^{14} – 1.0×10^{17} [38]
Core material	MDF	Cotton	Glass	Aluminum	Poplar Plywood	Acrylic
E (GPa)	3.59 [43]	-	68.95 [44]	68.0 [38]	6.96 – 8.55 [43]	3.30 [38]

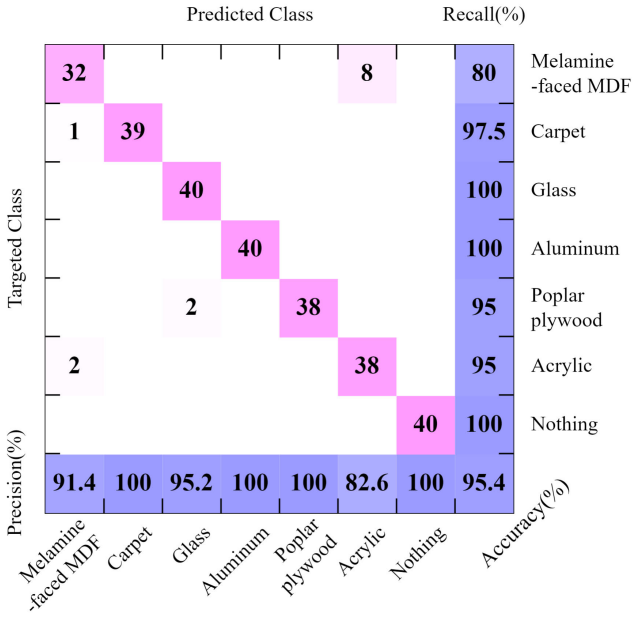

FIGURE 11. Classification confusion matrix of the trained dense neural network model.

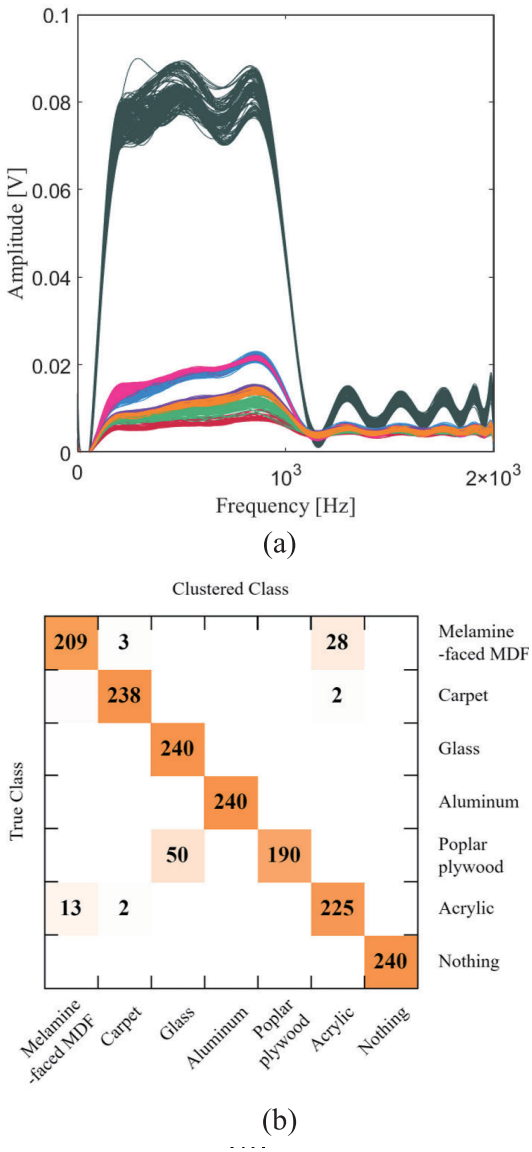

FIGURE 12. Segmentation results of k-means clustering (k = 7) using collected data: (a) frequency responses, and (b) clustering confusion matrix.

if they have different Young's modulus. This is because the ground is fixed to one side and there is little vibrating due to the actuator, so it is assumed that there will be no significant change in the sensor value. Thus, we speculated that resistivity and permittivity were more strongly affected than the Young's modulus.

B. ACCURACY OF CLASSIFICATION

To detect the floor panel materials, all processed data from dataset **D** were used in the proposed DNN classification model, as described in Section II-C. Prior to machine learning, 240 processed data per surface material were randomly split into training, test, and validation sets in a ratio of 4:1:1. After training was completed, the performance of the trained model was estimated using the validation set by calculating the values of recall, precision, and accuracy [48]. The results are illustrated in the confusion matrix shown in Fig. 11. As confirmed from this matrix, the overall accuracy of the classification model was 95.4%. The high accuracy confirmed the performance of our model. Herein, misclassification occurred in the melamine-faced

MDF. In reality, it showed a misprediction of the acrylic. This might have been caused by the similarities in the frequency responses of the materials. In particular, they have similar resistivity and Young's modulus values.

Furthermore, the k-means clustering method (k=7) was used on $\mathbf{x}_n$ (n = 1, …, 1680) of $\mathbf{D}$ to analyze the dataset from the perspective of unsupervised learning. The initial means were set to be the same as the average values in Fig. 9, and the mean square error (MSE) was used as the criterion for updating the k-means. The graphical results of the k-means clustering are shown in Fig. 12(a). After clustering, the clustered sets were mapped into classes according to the dominant corresponding $\mathbf{y}_n$ of $\mathbf{x}_n$ in the set. By mapping, the clustering results were statistically analyzed. Fig. 12(b) shows the accuracy of clustering with matrix. The k-means clustering method recorded a high accuracy of 93.0%; therefore, we verified the reliability of the obtained data. The high discriminability between different materials led to less overfitting during model training. However, 28 data of melamine-faced MDF were confused with the acrylic data, and 13 data of acrylic were confused with the melamine-faced MDF data. This could be because of the similarities in resistivity and Young's modulus values. In addition, 50 data for poplar plywood were clustered into a set of glass because these materials showed similar resistivity and dielectric constant values. Moreover, the performance of the DNN was compared with that of k-means clustering. The DNN accuracy was 2.4% higher than that of k-means clustering. Specifically, the confusion between glass and poplar plywood that appeared in k-means clustering was almost eliminated in the DNN model, and the confusion between acrylic and melamine-faced MDF was also reduced.

IV. CONCLUSION

In this study, a piezoelectric actuator–sensor pair and an artificial neural network were used to classify floor materials to enhance the performance of mobile robots. The actuator–sensor pair based on the PVDF film was fabricated to collect data from the floor. In addition, a suspension was used to maintain contact between the sensing system and the ground. Electrical systems for acquiring the sensor data were integrated into a mobile robot to create an isolated sensing environment. Extensive amounts of sensor data were collected through repetitive experiments and the data were processed using the HPF, FFT, and polynomial fitting. After training the DNN model with the processed data, seven floor materials were classified using the model, with a high accuracy of 95.4%. In addition, by investigating the effects of material properties on the sensor data, we confirmed that a lower resistivity or higher permittivity of the floor material might result in a higher peak value of the sensor responses. In addition, the collected data were verified using the k-means clustering method and showed 93.0% discriminability among classes, thereby demonstrating the reliability of the data.

However, we assumed and test flat and clean floor situations to observe whether the piezoelectric actuator–sensor pair could classify floor materials. Perhaps, it is difficult to predict floor materials when there is a lot of debris and uneven surfaces. To observe how this pair behaves in the real-life environment, further work will be conducted to investigate the impact on the pair by assuming various types of debris and terrain through force–displacement analysis. Moreover, to scrutinize the operation of the actuator-sensor pair and improve the classification performance, finite element analysis can be utilized, and the new data processing method can be adapted to point out the features of sensor data.

Consequently, the proposed method could be used to classify surface materials with high accuracy and to provide useful ground information for mobile robots. Furthermore, the proposed actuator–sensor pair can be used to collect material or texture information in a variety of applications such as autonomous robot cleaners or delivery robots.

ACKNOWLEDGMENT

The authors would like to thank Jiwon Jung for helps with drawing figures.

REFERENCES

[1] *Household Robots Market Size Global Report, 2022–2030*, Polaris Market Res., New York, NY, USA, 2022.
[2] P. Asgharian, A. M. Panchea, and F. Ferland, "A review on the use of mobile service robots in elderly care," *Robotics*, vol. 11, no. 6, p. 127, Nov. 2022.
[3] R. Raj and A. Kos, "A comprehensive study of mobile robot: History, developments, applications, and future research perspectives," *Appl. Sci.*, vol. 12, no. 14, p. 6951, Jul. 2022.
[4] T. Kataoka, "Robot and controlling method of the same," *J. Acoust. Soc. Amer.*, vol. 123, no. 1, p. 20, 2008.
[5] K. Almazrouei, I. Kamel, and T. Rabie, "Dynamic obstacle avoidance and path planning through reinforcement learning," *Appl. Sci.*, vol. 13, no. 14, p. 8174, Jul. 2023.
[6] C. Zong, Z. Ji, Y. Yu, and H. Shi, "Research on obstacle avoidance method for mobile robot based on multisensor information fusion," *Sensors Mater.*, vol. 32, no. 4, p. 1159, 2020.
[7] A. Milella, G. Reina, and M. Nielsen, "A multi-sensor robotic platform for ground mapping and estimation beyond the visible spectrum," *Precis. Agricult.*, vol. 20, no. 2, pp. 423–444, Apr. 2019.
[8] X. A. Wu, T. M. Huh, R. Mukherjee, and M. Cutkosky, "Integrated ground reaction force sensing and terrain classification for small legged robots," *IEEE Robot. Autom. Lett.*, vol. 1, no. 2, pp. 1125–1132, Jul. 2016.
[9] K. Walas, "Tactile sensing for ground classification," *J. Autom. Mobile Robot. Intell. Syst.*, vol. 7, no. 2, pp. 18–23, 2013.
[10] K. Kim, S. Kim, K. Lee, and S. Chae, "Robot cleaner for cleaning in consideration of floor state through artificial intelligence and operating method for the same," U.S. Patent 11 779 180 B2, Oct. 10, 2023.
[11] S. Wilson, J. Potgieter, and K. Arif, "Floor surface mapping using mobile robot and 2D laser scanner," in *Proc. 24th Int. Conf. Mechatronics Mach. Vis. Pract. (M2VIP)*, Nov. 2017, pp. 1–6.
[12] A. Milella, G. Reina, and J. Underwood, "A self-learning framework for statistical ground classification using radar and monocular vision," *J. Field Robot.*, vol. 32, no. 1, pp. 20–41, Jan. 2015.
[13] S. Zenker, E. E. Aksoy, D. Goldschmidt, F. Wörgötter, and P. Manoonpong, "Visual terrain classification for selecting energy efficient gaits of a hexapod robot," in *Proc. IEEE/ASME Int. Conf. Adv. Intell. Mechatronics*, Jul. 2013, pp. 577–584.
[14] A. Vicente, J. Liu, and G.-Z. Yang, "Surface classification based on vibration on omni-wheel mobile base," in *Proc. IEEE/RSJ Int. Conf. Intell. Robots Syst. (IROS)*, Sep. 2015, pp. 916–921.
[15] M. Evans, C. W. Fox, M. J. Pearson, and T. J. Prescott, "Spectral template based classification of robotic whisker sensor signals in a floor texture discrimination task," in *Proc. Towards Auto. Robot. Syst. (TAROS)*, 2009, pp. 19–24.

[16] C. A. Brooks and K. Iagnemma, "Vibration-based terrain classification for planetary exploration rovers," *IEEE Trans. Robot.*, vol. 21, no. 6, pp. 1185–1191, Dec. 2005.
[17] L. Zou, C. Ge, Z. Wang, E. Cretu, and X. Li, "Novel tactile sensor technology and smart tactile sensing systems: A review," *Sensors*, vol. 17, no. 11, p. 2653, Nov. 2017.
[18] Y. Peng, N. Yang, Q. Xu, Y. Dai, and Z. Wang, "Recent advances in flexible tactile sensors for intelligent systems," *Sensors*, vol. 21, no. 16, p. 5392, Aug. 2021.
[19] Y. Wan, Y. Wang, and C. F. Guo, "Recent progresses on flexible tactile sensors," *Mater. Today Phys.*, vol. 1, pp. 61–73, Jun. 2017.
[20] T.-D. Nguyen and J. S. Lee, "Recent development of flexible tactile sensors and their applications," *Sensors*, vol. 22, no. 1, p. 50, Dec. 2021.
[21] S. Kim, H. Shin, K. Song, and Y. Cha, "Flexible piezoelectric sensor array for touch sensing of robot hand," in *Proc. 16th Int. Conf. Ubiquitous Robots (UR)*, Jun. 2019, pp. 21–25.
[22] K. Shin, M. Sim, E. Choi, H. Park, J.-W. Choi, Y. Cho, J. I. Sohn, S. N. Cha, and J. E. Jang, "Artificial tactile sensor structure for surface topography through sliding," *IEEE/ASME Trans. Mechatronics*, vol. 23, no. 6, pp. 2638–2649, Dec. 2018.
[23] K. Shin, D. Kim, H. Park, M. Sim, H. Jang, J. I. Sohn, S. N. Cha, and J. E. Jang, "Artificial tactile sensor with pin-type module for depth profile and surface topography detection," *IEEE Trans. Ind. Electron.*, vol. 67, no. 1, pp. 637–646, Jan. 2020.
[24] Y. Wang, J. Chen, and D. Mei, "Flexible tactile sensor array for slippage and grooved surface recognition in sliding movement," *Micromachines*, vol. 10, no. 9, p. 579, Aug. 2019.
[25] B. Heyneman and M. R. Cutkosky, "Slip classification for dynamic tactile array sensors," *Int. J. Robot. Res.*, vol. 35, no. 4, pp. 404–421, Apr. 2016.
[26] J. Chung, H. Lim, M. Lim, and Y. Cha, "Object classification based on piezoelectric actuator-sensor pair on robot hand using neural network," *Smart Mater. Struct.*, vol. 29, no. 10, Oct. 2020, Art. no. 105020.
[27] Z. Gao, B. Ren, Z. Fang, H. Kang, J. Han, and J. Li, "Accurate recognition of object contour based on flexible piezoelectric and piezoresistive dual mode strain sensors," *Sens. Actuators A, Phys.*, vol. 332, Dec. 2021, Art. no. 113121.
[28] V. T. Rathod, D. R. Mahapatra, A. Jain, and A. Gayathri, "Characterization of a large-area PVDF thin film for electro-mechanical and ultrasonic sensing applications," *Sens. Actuators A, Phys.*, vol. 163, no. 1, pp. 164–171, Sep. 2010.
[29] N. Kirchner, D. Hordern, D. Liu, and G. Dissanayake, "Capacitive sensor for object ranging and material type identification," *Sens. Actuators A, Phys.*, vol. 148, no. 1, pp. 96–104, Nov. 2008.
[30] N. Srivastava, "Improving neural networks with dropout," *Univ. Toronto*, vol. 182, no. 566, p. 7, 2013.
[31] N. Srivastava, G. Hinton, A. Krizhevsky, I. Sutskever, and R. Salakhutdinov, "Dropout: A simple way to prevent neural networks from overfitting," *J. Mach. Learn. Res.*, vol. 15, pp. 1929–1958, Sep. 2014.
[32] X. Ying, "An overview of overfitting and its solutions," *J. Phys., Conf. Ser.*, vol. 1168, Feb. 2019, Art. no. 022022.
[33] S. Mutasa, S. Sun, and R. Ha, "Understanding artificial intelligence based radiology studies: What is overfitting?" *Clin. Imag.*, vol. 65, pp. 96–99, Sep. 2020.
[34] S. J. Nowlan and G. E. Hinton, "Simplifying neural networks by soft weight sharing," in *The Mathematics of Generalization*. Boca Raton, FL, USA: CRC Press, 1995, pp. 373–394.
[35] S. Gupta, R. Gupta, M. Ojha, and K. P. Singh, "A comparative analysis of various regularization techniques to solve overfitting problem in artificial neural network," in *Proc. Int. Conf. Recent Develop. Sci., Eng. Technol.*, 2018, pp. 363–371.
[36] L. Prechelt, "Early stopping—But when?" in *Neural Networks: Tricks of the Trade*, G. B. Orr, Ed. Cham, Switzerland: Springer, 1998, pp. 53–67.
[37] L. Prechelt, "Automatic early stopping using cross validation: Quantifying the criteria," *Neural Netw.*, vol. 11, no. 4, pp. 761–767, Jun. 1998.
[38] *Matweb*. [Online]. Available: https://www.matweb.com
[39] R. Pérez-Campos, J. Monzó-Cabrera, J. Fayos-Fernández, A. Díaz-Morcillo, A. Martínez-González, A. J. Lozano-Guerrero, J. L. Pedreño-Molina, and J. A. García-Gambín, "Dielectric characterization of fabric aggregates around the 2.45 GHz ISM band under various humidity, density, and temperature conditions," *Materials*, vol. 16, no. 12, p. 4428, Jun. 2023.
[40] N. P. Bansal and R. H. Doremus, *Handbook of Glass Properties*. New York, NY, USA: Academic, 1986.
[41] K. C. Varada Rajulu and B. N. Mohanty, "Dielectric and conductivity properties of some wood composites," *Int. J. Eng. Technol.*, vol. 8, pp. 51–60, Aug. 2016.
[42] E. Kasaw, A. Haile, and M. Getnet, "Conductive coatings of cotton fabric consisting of carbonized charcoal for e-textile," *Coatings*, vol. 10, no. 6, p. 579, Jun. 2020.
[43] Z. Cai and R. J. Ross, "Mechanical properties of wood-based composite materials," Dept. Agricult., Forest Products Lab., Madison, WI, USA, Tech. Rep. FPL-GTR-190, 2010.
[44] F. W. Preston, "The mechanical properties of glass," *J. Appl. Phys.*, vol. 13, no. 10, pp. 623–634, 2004.
[45] D.-S. Kim and J.-S. Lee, "Propagation and attenuation characteristics of various ground vibrations," *Soil Dyn. Earthq. Eng.*, vol. 19, no. 2, pp. 115–126, Feb. 2000.
[46] A. M. Thomas, K. R. Pradeep, and P. Mathew, "Structural health monitoring using piezoelectric sensors and actuators," *Appl. Mech. Mater.*, vol. 857, pp. 255–260, Nov. 2016.
[47] D. H. Wang and S. L. Huang, "Health monitoring and diagnosis for flexible structures with PVDF piezoelectric film sensor array," *J. Intell. Mater. Syst. Struct.*, vol. 11, no. 6, pp. 482–491, Jun. 2000.
[48] M. Grandini, E. Bagli, and G. Visani, "Metrics for multi-class classification: An overview," 2020, *arXiv:2008.05756*.

JIYONG MIN received the B.S. degree in electrical engineering from Hanyang University, Seoul, Republic of Korea, in 2021. He is currently pursuing the Ph.D. degree in electrical engineering with Korea University, Seoul. His research interests include flexible sensors and actuators, virtual reality, and robotics.

JISUNG PACK is currently pursuing the B.S. degree in electrical engineering with Korea University, Seoul, Republic of Korea.

HEON ICK PARK received the B.S. degree in electrical engineering from Kookmin University, Seoul, Republic of Korea, in 2022. He is currently pursuing the M.S. degree in electrical engineering with Korea University, Seoul. His research interest includes soft mechatronics.

YOUNGSU CHA (Senior Member, IEEE) received the B.S. degree in electrical engineering from Korea University, Seoul, South Korea, in 2004, the M.S. degree in electrical engineering from Korea Advanced Institute of Science and Technology (KAIST), Daejeon, South Korea, in 2007, and the Ph.D. degree in mechanical engineering from New York University, New York, NY, USA, in 2015. He was a Principal Research Scientist with the Center for Intelligent and Interactive Robotics, Korea Institute of Science and Technology (KIST), Seoul. He is currently an Associate Professor with the School of Electrical Engineering, Korea University. His research interests include smart materials and structures, multiphysics modeling, flexible sensors and actuators, energy harvesting, and robotics. He received the ASME Gary Anderson Early Achievement Award, in 2022.